THERMAL PROPERTIES OF SILICON NITRIDE BEAMS BELOW 1 KELVIN

G. Wang[1], V. Yefremenko[1], V. Novosad[1], A. Datesman[1], J. Pearson[1], G. Shustakova[1], R. Divan[2], C. Chang[3], J. McMahon[3], L. Bleem[3], A. T. Crites[3], T. Downes[3], J. Mehl[3], S. S. Meyer[3], and J. E. Carlstrom[3]

[1]Materials Science Division, Argonne National Laboratory
Lemont, Illinois, 60439, USA

[2]Center for Nanoscale Materials, Argonne National Laboratory
Lemont, Illinois, 60439, USA

[3]Kavli Institute for Cosmological Physics, the University of Chicago
Chicago, Illinois, 60637, USA

ABSTRACT

We have investigated the thermal transport of long, narrow beams of silicon nitride at cryogenic temperatures. Simultaneously employing a superconducting Transition Edge Sensor (TES) as both a heater and a sensor, we measured the thermal conductance of 1 μm thick silicon nitride beams of different lateral dimensions. Based upon these measurements, we calculate the thermal parameters of the beams. We utilize a boundary limited phonon scattering model and assume the phonon mean free path to be temperature independent in the calculation. In the temperature range from 300 mK to 530 mK, the following results are obtained for 20 (30) μm beams: the volume heat capacity is $0.083T+0.509T^3$ J/m^3-K, the width dependent phonon mean free path is 9.60 (11.05) μm, and the width dependent thermal conductivity is $5.60\times10^{-3}T+3.41\times10^{-2}T^3$ ($6.50\times10^{-3}T+3.93\times10^{-2}T^3$) W/m-K.

KEYWORDS: Phonon mean free path, heat capacity, thermal conductivity.

INTRODUCTION

Low stress silicon nitride (Si_3N_4) film has been widely used as mechanical supports and weak thermal links in cryogenic detectors. Despite many years of investigation and use, the thermal properties of Si_3N_4 film at low temperature are still not well understood,

particularly for long narrow Si_3N_4 beams. We investigate the thermal parameters of the beams using the width dependence of the thermal conductance with thermal test structures.

At low temperature, heat transport in an insulator is a process of phonon propagation. A consensus of Si_3N_4 heat transport is that there are a phonon radiative ballistic limit (also called surface specular reflection limit) and a Casimir [1] limit (also called diffusive limit) in a thin continuous Si_3N_4 film. Radiative ballistic phonon transport [2-4] appears at extremely low temperature, for example, below100 mK. The diffusive limit appears at much higher temperature [3]. Typically, the heat power flow as a function of bath temperature for a defined thermal structure is fitted as a power law [5, 6] of

$$P = K\left(T^n - T_b^{\,n}\right), \tag{1}$$

where T is the temperature at the hot end, T_b is the bath temperature, coefficient K and index n characterize thermal properties and phonon transport mechanism. The thermal conductance is the first derivative of the power over temperature,

$$G = nKT^{n-1}. \tag{2}$$

The index n approaches 4 both at the specular reflection limit and at the diffusive reflection limit. For long Si_3N_4 beams, the index n in the power law fit is generally less than 4 at a few hundred milli-Kelvin temperature, and the coefficient K could be significantly different at various cross section over beam length ratios. In principle, both K and n can be useful for extracting phonon mean free path. But due to the variation of index n for different tested devices, there is no specific model for the mean free path calculation so far.

In the phonon gas kinetic theory, thermal conductivity is written as

$$\kappa = (1/3)ClS, \tag{3}$$

where C is Si_3N_4 volume heat capacity, l is phonon mean free path, and S=6986 m/s is the average Si_3N_4 sound speed calculated with its longitudinal and transverse sound speeds [7]. The phonon mean free path could be much less than the beam length for a long narrow Si_3N_4 beam. Therefore, a phonon diffusive formulation can be used approximately for a description of heat transport. The heat flux is defined by Fourier's law,

$$q = -\kappa dT/dx, \tag{4}$$

where dT/dx is the temperature gradient along the Si_3N_4 beam. q is constant at a steady state. Therefore, the heat power from the hot end to the bath is

$$P = (A/L)\int_0^L q dx = -(AS/3L)\int_T^{T_b} CldT, \tag{5}$$

where L is the beam length, A is its cross section. For a defined thermal structure at a steady state, its thermal conductance can be written in the form of

$$G = AClS/3L. \tag{6}$$

For Si_3N_4, we may use amorphous material heat capacity [8, 9] in the form of

$$C = aT + bT^3, \tag{7}$$

where *a* and *b* are determined with experimental data. The departure from the Debye heat capacity in equation (7) is characteristic of the glass state of amorphous materials, such as Si_3N_4. Assuming a temperature independent phonon mean free path for simplicity, then the heat power from the hot end to the bath is

$$P = (B_1/2)\left(T^2 - T_b^{\,2}\right) + (B_2/4)\left(T^4 - T_b^{\,4}\right), \tag{8}$$

where

$$B_1 = (AS/3L)al, \tag{9}$$

and

$$B_2 = (AS/3L)bl. \tag{10}$$

Therefore, the power flow along the defined beams depends on temperatures at the hot end and of the bath, cross section over length ratio, phonon mean free path, volume heat capacity, and sound speed. To investigate thermal conductance of Si_3N_4, we made thermal test structures with TES. We use the TES as both a heater and a temperature sensor to measure the TES Joule power and bath temperature relation. We fit the data in two ways. One is a power law fit using equation (1). Another is a temperature independent mean free path fit using equation (8). We calculate the temperature independent phonon mean free path, volume heat capacity, and thermal conductivity of Si_3N_4 beams with the measured thermal conductance data and a boundary limited phonon scattering model.

THERMAL TEST STRUCTURES AND EXPERIMENTAL DATA

The thermal test structure, which consists of an island in the middle and four supporting Si_3N_4 beams, is shown in FIGURE 1. The device fabrication is performed at the

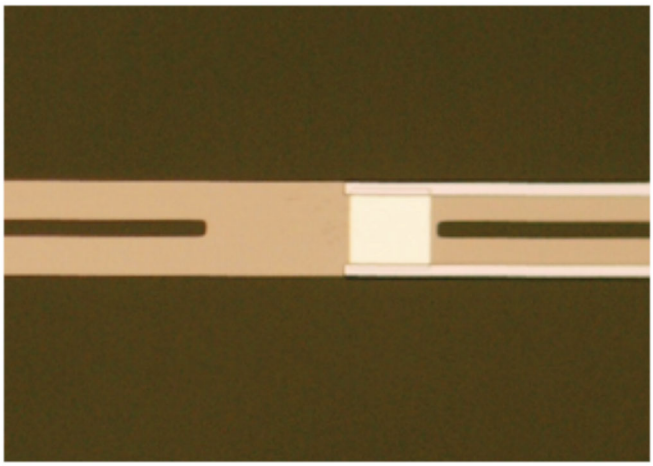

FIGURE 1. Thermal test structure. The middle island is 140 μm by 70 μm. The width of Si_3N_4 supporting beams is 30 μm (device #1 and #2) or 20 μm (device #3 and #4), and the length is 1380 μm. On the right side of the middle island is a Mo/Au bi-layer TES with two 10 μm wide and 120 nm thick Nb leads. On the left side of the middle island is a space for a heater in later experiments.

Materials Science Division and at the Center for Nanoscale Materials, Argonne National Laboratory. We purchased from Rogue Valley Microelectronics commercial 250 μm thick silicon wafers with 1 μm thick LPCVD low stress silicon nitride film on the surface. First we fabricate the Mo/Au bi-layer TES with DC magnetron sputtering and standard photon lithography techniques. The Mo is 28 nm thick, and Au is 30 nm thick. The 10 μm wide and 120 nm thick Nb leads are patterned with lift-off. The silicon behind the membrane in a 3 mm × 3 mm area is removed by KOH etching. The long Si_3N_4 beams are patterned with Reactive Ion Etch (RIE).

The TES, which has a normal resistance about 0.85 Ω, is used as both a heater and a temperature sensor for the thermal conductance measurement of the Si_3N_4 beams. At various bath temperatures, we measure TES I-V curves. The TES is operated with a shunt resistor of 8.6 mΩ. The TES current is read out with a NIST SQUID array. The TES resistance and Joule heating power as a function of its bias voltage are calculated with the I-V curves. When the TES is biased in its transition from normal into superconducting, its Joule heating power is nearly constant due to the strong negative electro-thermal feedback effect. For our measurements, we chose a TES resistance at 60% of its normal resistance in the transition range for computing Joule heating power. We call the fit temperature value at this resistance as Tc in TABLE 1. During the course of the measurement, the TES bias voltage changes slowly to keep the detector isothermal. Under this condition, the thermalized Si_3N_4 middle island in FIGURE 1 has approximately the same temperature as the TES. Therefore, at a thermal quasi-steady state, thermal power along the supporting Si_3N_4 beams, which equals TES Joule heating power, is a function of bath temperature.

For the thermal conductance measurement data, we fit the TES Joule heating power as a function of bath temperature both with a power law using equation (1) and with a temperature independent mean free path formulation using equation (8). For device #3, the mean free path fit is the solid line in FIGURE 2. The parameters Tc, B_1 and B_2 using equation (8) are found using a least square fit to minimize the fit error. The power law fit is the dashed line, which is shifted up by 10 pW for clarity. The parameters Tc, K and n using equation (1) are found using a least square fit. There is no observed Tc difference in the two methods. The width of the thermal test structures and the fit thermal parameters for four measured devices are summarized in TABLE 1.

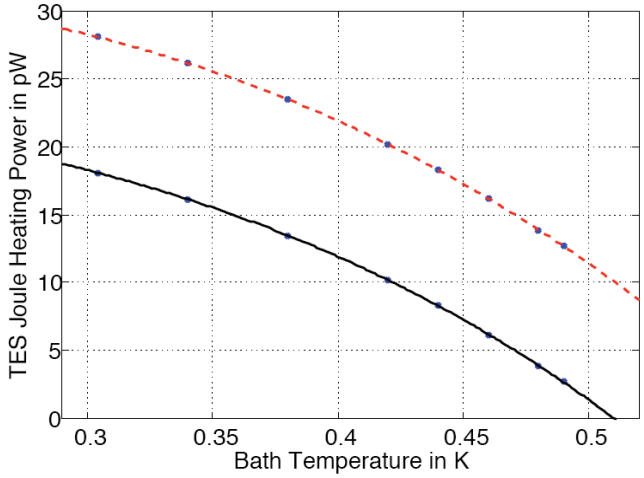

FIGURE 2. TES Joule heating power as a function of bath temperature. The dots are experimental data. The lower curve is the temperature independent phonon mean free path fit, which has a standard deviation of 2.8×10^{-2} pW. The upper curve is the power law fit, which has a standard deviation of 3.0×10^{-2} pW. The data and curve are shifted up by 10 pW for a clear visualization in the power law fit.

TABLE 1. Si_3N_4 thermal test structure beam width and the fit thermal parameters using equations (1) and (8).

Devices	W (μm)	Tc (K)	n	K (10^{-10} W/K^n)	B_1 (10^{-10} W/K^2)	B_2 (10^{-9} W/K^4)	B_2/B_1 (K^{-2})
Dev#1	30	0.510	2.95	2.99	1.89	1.08	5.71
Dev#2	30	0.525	3.03	3.24	1.86	1.20	6.45
Dev#3	20	0.513	3.02	1.74	1.01	0.65	6.13
Dev#4	20	0.530	2.90	1.78	1.18	0.67	5.68

In TABLE 1, the ratio of B_2 (or B_1, or nK^{n-1} at 0.4 K) for 30 μm beams and for 20 μm beams is 1.73 (or 1.71, or 1.74) instead of 1.5, which is the beams cross section ratio. Our experimental data agree with the published JPL data [12]. For the same Si_3N_4 thickness and length, JPL results show that the thermal conductance of 9 μm wide beams is slightly larger than 3 times that of 3 μm wide beams at a temperature of 0.4 K, but the thermal conductance of 135 μm wide beams is significantly larger than 15 times that of 9 μm wide beams. In the following data interpretation, we use the ratio between the average values of B_2 for 30 μm beams and for 20 μm beams as a typical number to interpret our data for a mean free path evaluation. Second, B_2/B_1, which is equivalent to b/a in equation (7), is around 6 K^{-2} for all the four devices. This value, which may correlate to the index n in the power law fit, is typical for amorphous materials heat capacity at low temperatures [8].

We note that there are several error sources in the measurements. First, there are uncertainties of thickness and width of the Si_3N_4 beams. The thickness uncertainty is less than 3%, and the width uncertainty due to micro-fabrication is less than 0.5 μm. Second, the uncertainty of the shunt resistor's value is ±0.1 mΩ, which gives a TES Joule heating power error less than 2%. Third, the TES resistance could depend on its current at various bath temperatures. We found that the temperature shift could be up to 0.5 mK/μA at the low resistance end of the TES, but could be less than 0.1 mK/μA at the high resistance end. We chose a TES resistance at 60% of its normal value for Joule heating power calculation. The estimated temperature error at the same TES resistance for a bath at temperature of 300 mK and of 500 mK is less than 2 mK. Furthermore, the Si_3N_4 island temperature should be used for the beams thermal conductance calculation. The thermal power exchange between TES and Si_3N_4 film depends on their temperatures [10, 11],

$$P_{ep} = \Sigma\Lambda\left(T_{TES}{}^5 - T_{SiN}{}^5\right), \tag{11}$$

where Σ is TES film volume, and Λ is electron-phonon coupling strength, which has a typical value of 1×10^9 W/m^3-K^5. To count the linear term only, the temperature difference between the TES and the Si_3N_4 island is less than 1 mK for the low thermal conductance devices. Lastly, the superconducting Nb leads contribute about 2~3% volume and are treated as the same as the Si_3N_4, because we did not see any apparent thermal conductivity difference in other tests by changing the width of the leads by a factor of 2. In summary, the estimated overall error in the thermal conductance measurements is less than 10%.

BOUNDARY LIMITED PHONON SCATTERING

According to equations (3) and (8), a plausible solution for the thermal conductance ratio of 1.73 is that the mean free path for 30 μm beams is 15% larger than that for 20 μm

beams. To estimate the phonon mean free path, we use the boundary limited phonon scattering model [13, 14]. For a sample with large side ratio, the boundary diffusive reflection limited phonon mean free path [13] is

$$l_B = (3W/2n)\left[n^3 I(1/n) + I(n)\right], \tag{12}$$

where the sample has sides of W and nW, and

$$I(n) = (n/2)\sinh^{-1}(n) + (1/6)\left[\left(1+n^2\right)^{0.5}\left(n^2-2\right) + \left(2-n^3\right)\right]. \tag{13}$$

With a fraction of diffusive reflection f, the phonon mean free path [13] is

$$l = \frac{3W}{2n}\sum_0^\infty f(1-f)^J \left\{ \begin{array}{l} n^3\left[(J+1)^3\left(\frac{1}{n(J+1)}\right) - J^3 I\left(\frac{1}{nJ}\right)\right] \\ +\frac{1}{2}(2-\delta_{J,0})\left[I(n(J+1)) - 2I(nJ) + I(n(J-1))\right] \end{array} \right\}, \tag{14}$$

where J is the number of times a particular phonon impinges on the surface before being diffusely scattered. The Kronecker delta function ensures that a correct phonon counting procedure is made. Eddison and Wybourne [14] describe in detail how the phonon mean free path changes with the diffusive scattering probability at surface when the two narrow sides of the samples are treated for a complete diffusive scattering due to the edge's roughness. We apply the model to our thermal test structure data because of the similarity of the model and our devices. The diffusive reflection fraction dependent phonon mean free paths for 30 μm beams and for 20 μm beams are shown in FIGURE 3. The phonon mean free paths increase rapidly with a decrease of diffusive reflection fraction when a specular phonon reflection limit is approached. The mean free path ratio of phonons between 30 μm beams and 20 μm beams depends on the fraction of phonon diffusive reflection at the surface, as is shown in the inset of FIGURE 3.

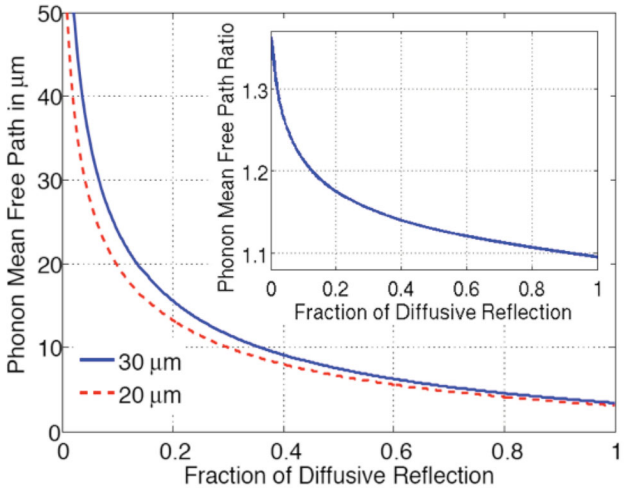

FIGURE 3. Phonon mean free path as a function of fraction of phonon diffusive reflection for 1 μm thick Si_3N_4 beams of 30 μm wide (solid line) and of 20 μm wide (dashed line). At a 100% diffusive reflection, the phonon mean free path is 3.45 (3.15) μm for 30 (20) μm beams. The inset shows phonon mean free path ratio between 30 μm and 20 μm beams. Phonon boundary scattering model [13, 14] is used for the calculation.

Using FIGURE 3 as a lookup table, we find that the fraction of phonon diffusive reflection is about 32% for a 15% phonon mean free path difference between 30 μm beams and 20 μm beams. Therefore, the mean free path is 11.05 μm for 30 μm beams, and is 9.60 μm for 20 μm beams. Using these mean free paths and equation (9), the average value of a is approximately 0.083 J/m^3-K^2 both for 30 μm beams and for 20 μm beams. The average value of b is approximately 0.509 J/m^3-K^4 both for 30 μm beams and for 20 μm beams using equation (10). As a comparison, the Debye volume heat capacity for a crystal solid at a low temperature is a cubic function of temperature [15]. In SI units, it is

$$C \approx \left(16\pi^5/5\right)\left(k_B{}^4/h^3S^3\right)T^3 \approx 0.359T^3, \tag{15}$$

where k_B is Boltzmann constant, and h is Plank constant. In our data, the Si_3N_4 volume heat capacity is $0.083T+0.509T^3$ J/m^3-K, which is about 3 times the Debye heat capacity in the interested temperature. This heat capacity is typical for amorphous materials [8, 9].

The Si_3N_4 beams thermal conductivity can be calculated with equation (3). The thermal conductivity is $6.50\times10^{-3}T+3.93\times10^{-2}T^3$ W/m-K for 1 μm thick and 30 μm wide Si_3N_4 beams, and $5.60\times10^{-3}T+3.41\times10^{-2}T^3$ W/m-K for 20 μm beams.

With the estimated phonon mean free paths, we can calculate the expected surface roughness of the Si_3N_4. The surface diffusive scattering probability [16] is

$$f = 1-\exp(-16\pi^3\eta^2/\lambda_D{}^2), \tag{16}$$

where η is RMS value of surface roughness, and λ_D is the phonon domain wavelength [17], which is inversely proportional to temperature,

$$\lambda_D = 0.235hS/k_BT. \tag{17}$$

According to [16], the temperature dependent mean free path could be calculated for a thermal structure with a length larger than its lateral dimension with a formula

$$l(T) = l_B(2-f)/f, \tag{18}$$

where l_B is defined in equation (12). The temperature averaged mean free path is

$$l = \int_{T_b}^{T_C} l(T)dT/(T_C - T_b), \tag{19}$$

where T_C is the TES temperature, which approximately equals to the temperature of the Si_3N_4 middle island in FIGURE 1. We can plot the phonon mean free path l versus the surface roughness η relation using equations (16), (17), (18), and (19). We find that the Si_3N_4 beams surface RMS roughness in our thermal test structures is 7.2 nm for 30 μm beams with l=11.05 μm, and is 7.4 nm for 20 μm beams with l=9.60 μm. The difference is 0.2 nm, which is certainly in the allowed error range of the experimental data.

CONCLUSION

The phonon mean free path in narrow Si_3N_4 beams, as well as the dependence of this parameter upon beam dimension and surface roughness, is a key parameter enabling

successful thermal design of cryogenic bolometric detectors. To our knowledge, this paper contains the first calculation of the phonon mean free path of Si_3N_4 beams extracted from experimental results below 1 Kelvin. A boundary limited phonon scattering model was utilized to calculate the volume heat capacity, phonon mean free path, thermal conductivity, and surface roughness of our lithographically defined suspended Si_3N_4 structures. The calculated value of the volume heat capacity using our thermal conductance data agrees with the volume heat capacity expected for amorphous materials.

ACKNOWLEDGEMENTS

The authors wish to acknowledge the support from the NIST Quantum Sensors Group at Boulder for providing SQUID arrays, and to thank Matthew E. Kenyon at JPL for suggestions in devices fabrication. The work at Argonne National Laboratory, including the use of facility at the Center for Nanoscale Materials, was supported by the U.S. Department of Energy, under Contract No. DE-AC02-06CH11357. The work at the University of Chicago is supported by the National Science Foundation through grant ANT-0638937 and the NSF Physics Frontier Center grant PHY-0114422 to the Kavli Institute of Cosmological Physics at the University of Chicago. It also receives generous support from the Kavli Foundation and the Gordon and Betty Moore Foundation.

REFERENCES

1. Casimir, H. B. G., *Physica* **5,** pp. 495-500 (1938).
2. Hoevers, H. F. C., Ridder, M. L., Germeau, A., Bruijn, M. P., de Korte, P. A. J., and Wiegerink, R. J., *Applied Physics Letters* **86**, pp. 251903 (2005).
3. Holmes, W., Gildemeister, J. M., Richards, P. L., and Kotsubo, V., *Applied Physics Letters* **72**, pp. 2250-2252 (1998).
4. Klitsner, T., VanCleve, J. E., Fischer, H. E., and Pohl, R. O., *Physical Review B* **38**, pp.7576-7594 (1988).
5. Kenyon, M., Day, P. K., Bradford, C. M., Bock, J. J., and Leduc, H. G., *Journal of Low Temperature Physics* **151**, pp. 112-118 (2008).
6. Rostem, K., Glowacka, D., Goldie, D. J., and Withington, S., *Journal of Low Temperature Physics* **151**, pp. 76-81 (2008).
7. Bruls, R. J., Hintzen, H. T., de With, G., and Metselaar, R., *Journal of the European Ceramic Society* **21**, pp. 263-268 (2001).
8. Zeller, R. C. and Pohl, R. O., *Physical Review B* **4**, pp. 2029-2041 (1971).
9. Stephens, R. B., *Physical Review B* **8**, pp. 2896-2905 (1973).
10. Wellstood, F. C., Urbina, C., and Clarke, J., *Physical Review B* **49**, pp. 5942 (1994).
11. Savin, A. M., Pekola, J. P., Averin, D. V., and Semenov, V. K., *Journal of Applied Physics* **99**, pp. 084501 (2006).
12. Kenyon, M., Day, P. K., Bradford, C. M., Bock, J. J., and Leduc, H. G., *Proc. SPIE* **6275**, pp. 627508 (2006).
13. Wybourne, M. N., Eddison, C. G., and Kelly, M. J., *Journal of Physics C: Solid State Physics* **17**, pp. L607-L612 (1984).
14. Eddison, C. G. and Wybourne, M. N., *Journal of Physics C: Solid State Physics* **18**, pp. 5225-5234 (1985).
15. Ashcroft, N. W. and Mermin, N. D., *Solid State Physics*, Harcourt Brace College Publishers, Fort Worth, 1976, pp. 457.
16. Ziman, J. M., *Electrons and Phonons*, Oxford University Press, Oxford, 1979, pp. 456.
17. Pohl, R. O. and Liu, X., *Reviews of Modern Physics* **74**, pp. 991-1013 (2002).